Journal of Industrial and Engineering Chemistry 17 (2011) 198–207

Contents lists available at ScienceDirect

Journal of Industrial and Engineering Chemistry

journal homepage: www.elsevier.com/locate/jiec

Reduction in CO emissions along a two-stage hydrogen-permselective membrane reactor in methanol synthesis process

M.R. Rahimpour *, M.S. Baktash, B. Vaferi, S. Mazinani

Chemical Engineering Department, School of Chemical and Petroleum Engineering, Shiraz University, Shiraz 71345, Iran

ARTICLE INFO

Article history:
Received 18 May 2010
Accepted 13 July 2010
Available online 19 February 2011

Keywords:
CO removal
Hydrogen-permselective membrane
Two-stage membrane reactor
Dynamic model
Catalyst deactivation

ABSTRACT

Carbon monoxide (CO) is a scentless and invisible gas that is quite poisonous. It is also known to be a major environmental pollutant. Industrial chemical processes contribute to CO pollution levels in the atmosphere. One of the most important processes for controlling the carbon monoxide content is conversion of CO to methanol by catalytic hydrogenation. The present work investigates enhancement of CO conversion in a conventional two-stage methanol synthesis reactor using a hydrogen-permselective membrane. For this membrane system, a one-dimensional dynamic plug flow model was proposed in the presence of long-term catalyst deactivation. This model compares CO removal in a membrane two-stage methanol synthesis reactor with a conventional two-stage methanol synthesis reactor. A conventional two-stage reactor is a vertical shell and tube in which the first reactor coolant is saturated water and the second one is cooled with synthesis gas. In a membrane two-stage reactor, the wall of the tubes in the gas-cooled reactor is coated with a Pd–Ag membrane, which only permits the diffusion of hydrogen. For validation of the recommended dynamic model, the measured daily process data of a methanol plant recorded for a period of 4 years were used and a good agreement was obtained.

1. Introduction

Carbon monoxide (CO) is a colorless, odorless and toxic gas that even at low levels of exposure is very dangerous for human health and environment. CO can starve critical body organs, especially the brain and heart, of oxygen. Once inside the lungs, CO molecules pass easily into the bloodstream and compete with oxygen for hemoglobin in the red blood cells. In addition, the industrial applications of environmental technology have increased and reduction in CO concentration can significantly counteract the growth of CH_4 in the atmosphere, so it has important indirect effects on global warming [1,2]. To minimize these effects, the carbon monoxide emissions from industrial sources have to be decreased. One possible approach is recycling and fixing CO in a chemical process to form useful products such as methanol which is regarded as the effective method to reduce carbon monoxide concentration in the atmosphere. Methanol is widely used as a feedstock for the production of chemicals and is considered as a viable source for the generation of hydrogen for fuel cell application. It is a suitable fuel to produce hydrogen by steam reforming because of low operating temperatures (250–300 °C), low expense, simple to storage and eminent miscibility with water. Hydrogen plays a major role in the future as a carbon-free fuel for installing H_2 reforming unit to a portable fuel cell, compact design of reformer is mainly the strategic point [3–6]. Commercially, methanol can be recovered from many resources and is produced by catalytic conversion of synthesis gas in large scale. Synthesis gas consists of CO, CO_2, and H_2 and some inert components like CH_4 and N_2.

At the entrance of the methanol reactor, the reactions are rate base, so increasing temperature enhances rate of reaction and CO conversion, but at the end of reactor, the reactions are equilibrium base and increasing temperature, decreases CO equilibrium conversion. Therefore, in order to reach the highest removal rate of CO, implementing a higher temperature at the entrance of the reactor and then reducing temperature gradually towards the exit of reactor is one of the significant issues in methanol synthesis reactor.

Recently, a two-stage methanol synthesis reactor was introduced by Lurgi instead of a single-type for CO conversion to methanol [7]. This system is an advanced technology for converting synthesis gas to methanol at low cost and in large quantities. The configuration of this system is based on the two-stage reactor system. The first is a high temperature water-cooled reactor that is combined in series with a low temperature gas-cooled reactor and partial conversion of CO to methanol is

* Corresponding author. Tel.: +98 76 2303071; fax: +98 76 6287294.
E-mail address: rahimpor@shirazu.ac.ir (M.R. Rahimpour).

1226-086X/$ – see front matter © 2011 The Korean Society of Industrial and Engineering Chemistry. Published by Elsevier B.V. All rights reserved.
doi:10.1016/j.jiec.2011.02.001

accomplished in this reactor. Reacting gas composition in the second reactor is essentially poor in H_2, so performance of this reactor is lower than first reactor and decreases system efficiency. One way to reach higher conversion of CO to methanol is the addition of hydrogen to the reacting gas selectively by using membrane in gas-cooled reactor that leads to a shift of the chemical equilibrium towards the product side [8].

A membrane two-stage methanol synthesis reactor is a modified system which combines the chemical and membrane conversion in one system [9]. The main advantages of this system are: enhancement of CO conversion, overcoming with the potential limitations imposed by thermodynamic equilibrium [8], improvement of kinetics-limited reactions in the first reactor due to the higher feed temperature, enhancement of equilibrium limited reactions due to a lower temperature in the gas-cooled reactor and control of stoichiometric number of reacting gases along the second reactor by hydrogen diffusion through the membrane. The membrane separation is governed by both the chemical nature of the membrane material and the physical structure of the membrane [10]. Membrane conversion technology in chemical reaction processes is mainly used in reaction systems containing hydrogen and oxygen, and is based on inorganic membranes [11]. It was observed that diffusion of hydrogen through palladium membranes can enhance the selectivity of hydrogenation [12]. The use of Pd membranes is hindered because palladium shows a transition from the α-phase (hydrogen poor) to the β-phase (hydrogen rich) at temperatures below 300 °C and pressures below 2 MPa, depending on the hydrogen concentration in the metal. Since the lattice constant of the α-phase is 3% smaller than that of the β-phase this transition leads to lattice strain, and consequently after a few cycles, to a deformity of the metal lattice [13]. In many hydrogen-related reaction systems, Pd-alloy membranes on a stainless steel support were used as the hydrogen-permeable membrane [14]. A maximum value of hydrogen permeability is reached for an alloy with composition of 23 wt% silver [15].

For decades, palladium-based membranes have been used in transport of hydrogen because of their high permeability, good surface properties and 100% hydrogen selectivity [16]. These membranes combine hydrogen transition with distinguishing properties such as resistance to high temperatures, solvents, and corrosion. The main cause of the Pd-based membranes development is: low costs as well as perm-selectivity combined with good mechanical, thermal and long-term stability [17]. These properties make interesting use of palladium-based membranes such as Pd–Ag membranes in petrochemical industry.

There is one study on conversion of CO to methanol in Pd–Ag membrane single-type methanol synthesis reactor [8], but no investigation regarding the use of a Pd-membrane in two-stage methanol synthesis reactor for enhancement of CO conversion. Therefore, it was decided to first study on this system.

The aim of present work is reduction of carbon monoxide emission in a conventional two-stage methanol synthesis reactor. In this system, the walls of tubes in the gas-cooled reactor are covered with a layer of hydrogen perm-selective membrane. The driving force for hydrogen diffusion is its partial pressure gradient from feed synthesis gas to the reacting gas. The advantages of this concept will be discussed based on temperature, activity of catalyst and concentration profiles. The results are compared with the performance of conventional two-stage methanol synthesis reactor.

2. Process description

2.1. Conventional two-stage methanol synthesis reactor

Schematic diagram of a conventional two-stage methanol synthesis reactor is shown in Fig. 1.

The catalyst is packed in shell side of water-cooled reactor and vertical tubes of gas-cooled reactor. Reactions of methanol synthesis are performed over commercial $CuO/ZnO/Al_2O_3$ catalyst. Cold feed synthesis gas is fed to tubes of the second reactor and is flowing in counter-current mode with methanol-containing reacting gas in the shell of this reactor. Then outlet synthesis gas is entered to tubes of the first reactor and chemical reaction initiated by catalyst. The remaining heat of reaction is transferred to the cooling water inside the shell. In this stage, CO is partly converted to methanol. Then reacting gas mixture is left directing to the catalyst shell side of second reactor and its temperature is continuously reduced through the catalyst bed. Finally, the product is removed from the side stream of second reactor.

Temperature of the first reactor is higher than second reactor so the main catalyst deactivation occurs in this reactor. Therefore, the lower operating temperature in the gas-cooled reactor results in a practically unlimited catalyst service life. In addition, reaction control extends catalyst life time of the water-cooled reactor.

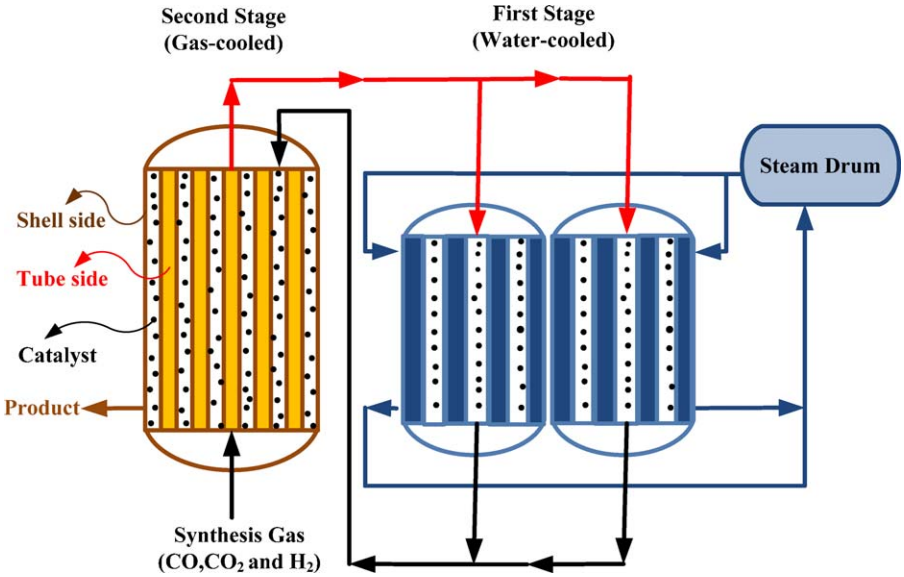

Fig. 1. Schematic flow diagram of conventional two-stage methanol synthesis reactor.

Table 1
Specifications of catalyst and reactors of conventional two-stage methanol synthesis.

Water-cooled reactor		Gas-cooled reactor	
Parameter	Value	Value	Unit
D	4.5	5.5	[m]
D_i	40.3	21.2	[mm]
D_o	4.5	25.4	[mm]
d_p	0.00574	0.00574	[m]
ρ_s	1770	1770	[kg m^{-3}]
c_{ps}	5.0	5.0	[kJ kg^{-1} K^{1}]
λ_c	0.004	0.004	[W m^{-1} K^{-1}]
a_v	625.7	625.7	[m^2 m^{-3}]
ε_s	0.39	0.39	
ε_B	0.39	0.39	
Tube length	8	10	[m]
Number of tubes	5955	3026	
Shell side pressure	–	71.2	[bar]
Tube side pressure	75	76.98	[bar]

Table 2
Input data of the conventional two-stage methanol synthesis reactor.

Feed conditions	Value
Feed composition (mol%)	
CO	8.68
CO_2	8.49
H_2	64.61
CH_4	9.47
N_2	8.2
H_2O	0.1
CH_3OH	0.37
Argon	0.24
Inlet temperature (K)	401
Total molar flow rate per tube (mol s^{-1})	7.1
Pressure (bar)	76

The input data and industrial design of the catalyst pellet for the conventional two-stage methanol synthesis reactor have been listed in Tables 1 and 2.

2.2. Membrane two-stage methanol synthesis reactor

Fig. 2 shows the schematic diagram of a membrane two-stage methanol synthesis reactor configuration for CO conversion. Procedure of membrane system is similar to conventional two-stage methanol synthesis reactor, with the exception that in this system, the walls of tubes in the gas-cooled reactor are coated with a hydrogen perm-selective membrane. The pressure difference between the shell (71.2 bar) and tubes (76.98 bar) permits the hydrogen diffusion through the Pd–Ag membrane layer. On the other hand, in the new system, mass and heat transfer process simultaneously occurs between the shell and tube, while in the conventional-type only a heat transfer process occurs between them.

The membrane specifications are listed in Table 3. Also, all specifications for the membrane two-stage system in the first and second methanol synthesis reactors are the same as of the conventional methanol synthesis reactor summarized in Tables 1 and 2.

3. Mathematical model

The mathematical model for the simulation of membrane two-stage methanol synthesis reactor was developed based on the following assumptions:

(1) One-dimensional plug flow;
(2) Axial dispersion of heat is negligible compared with convection;
(3) Gases are ideal;
(4) Radial diffusion in the catalyst pellet is neglected;
(5) There are no radial concentration and temperature gradients;
(6) The axial diffusion of hydrogen through the membrane is neglected compared to the radial diffusion;

In Fig. 3 an elemental of length Δz is considered.

3.1. Water-cooled reactor

In tube side mass and energy balance for solid phase are expressed by:

$$\varepsilon_s c_t \frac{\partial y_{is}^{tu}}{\partial t} = k_{gi}(y_i^{tu} - y_{is}^{tu}) + \eta r_i \rho_B a, \quad i = 1, 2, \ldots, N-1 \tag{1}$$

$$\rho_B c_{ps} \frac{\partial T_s^{tu}}{\partial t} = a_v h_f (T^{tu} - T_s^{tu}) + \rho_B a \sum_{i=1}^{N} \eta r_i (-\Delta H_{f,i}) \tag{2}$$

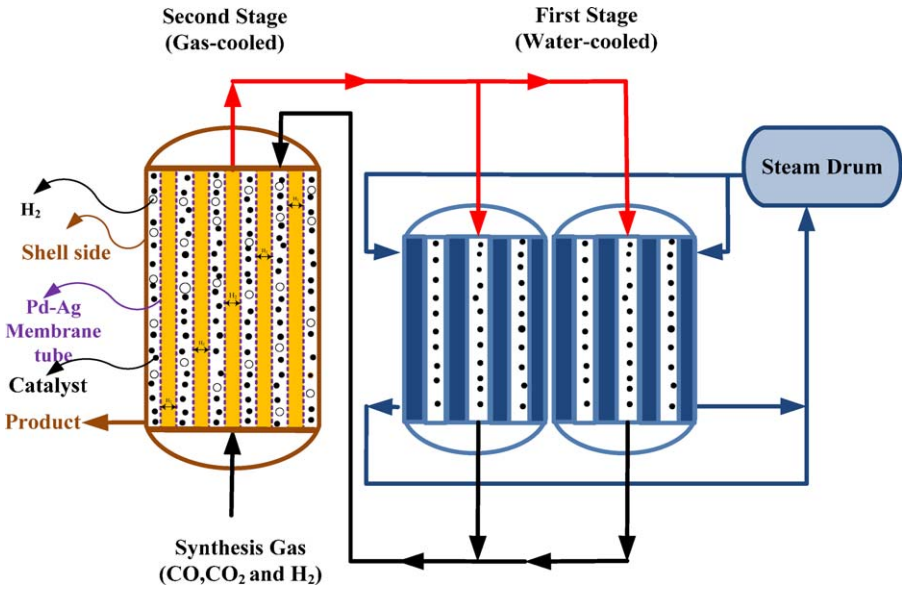

Fig. 2. Schematic flow diagram of membrane two-stage methanol synthesis reactor.

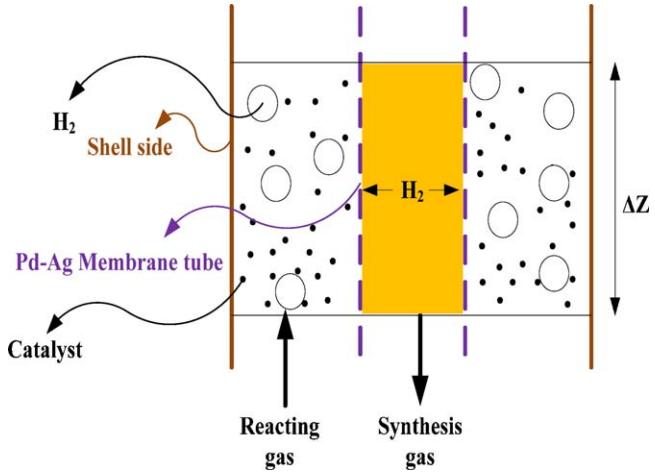

Fig. 3. Schematic diagram of an elemental volume of the second reactor in membrane two-stage system.

where y_{is}^{tu} and T_s^{tu} are the mole fraction and temperature of solid-phase in tube side, respectively, and i represents CH_3OH, CO, CO_2, H_2, H_2O. Argon, nitrogen and methane are inert components. The following two conservation equations are written for the fluid phase:

$$\varepsilon_B c_t \frac{\partial y}{\partial t} = -\frac{F^{tu}}{A_c}\frac{\partial y_i^{tu}}{\partial z} + a_v c_t k_{gi}(y_{is}^{tu} - y_i^{tu}), \quad i = 1, 2, \ldots, N-1 \tag{3}$$

$$\varepsilon_B c_t c_{pg}\frac{\partial T^{tu}}{\partial t} = -\frac{F^{tu}}{A_c}\frac{\partial T^{tu}}{\partial z} + a_v h_f(T_s^{tu} - T^{tu}) + \frac{\pi D_i}{A_c}U^{sh}(T^{sh} - T^{tu}) \tag{4}$$

where y_i^{tu} and T^{tu} are the fluid-phase mole fraction and temperature in tube side, also F^{tu} and A_c are total molar flow rate and cross-section in each tube, respectively. The boundary conditions are unknown and the more details are clarified in numerical solution.

$$z = 0; \quad F^{tu} = F, \quad y^{tu} = y_{i_{in}}, \quad T^{tu} = T_{in} \tag{5}$$

The initial conditions are:

$$t = 0; \quad y_i^{tu} = y_i^{ss}, \quad y_{is}^{tu} = y_{is}^{ss}, \quad T^{tu} = T^{ss}, \quad T_s^{tu} = T_s^{ss}, \quad a = 1 \tag{6}$$

3.2. Gas-cooled reactor

3.2.1. Shell side

Overall mass balance:

$$\varepsilon_B \frac{\partial c_t}{\partial t} = -\frac{1}{A^{sh}}\frac{\partial F^{sh}}{\partial z} + \frac{\alpha_H}{A^{sh}}(\sqrt{P_H^{tu}} - \sqrt{P_H^{sh}}) \tag{7}$$

where c_t, F^{sh} are total concentration and flow rate of reacting gas mixture in shell side. A^{sh} is cross-sectional area of shell and α_H is rating constant of hydrogen permeation. P_H^{tu} and P_H^{sh} are partial pressure of hydrogen in tube and shell sides, respectively. The mass and energy balance in the gas-cooled reactor for solid phase are the same as water-cooled reactor. The following equations are written for fluid phase:

$$\varepsilon_B c_t \frac{\partial y_i^{sh}}{\partial t} = -\frac{1}{A^{sh}}\frac{\partial F_i^{sh}}{\partial z} + a_v c_t k_{gi}(y_{is}^{sh} - y_i^{sh}) + \frac{\alpha_H}{A^{sh}}(\sqrt{P_H^{tu}} - \sqrt{P_H^{sh}}), \quad i = 1, 2, \ldots, N-1 \tag{8}$$

Table 3
Membrane specifications.

Parameter	Value	Unit
R_i	0.027	[m]
R_o	0.027008	[m]
δ	0.8×10^{-6}	[m]

$$\varepsilon_B c_t c_{pg}\frac{\partial T^{sh}}{\partial t} = -\frac{1}{A^{sh}}C_{pg}\frac{\partial(F^{sh}T^{sh})}{\partial z} + a_v h_f(T_s^{sh} - T^{sh}) + \frac{\alpha_H}{A^{sh}}(\sqrt{P_H^{tu}} - \sqrt{P_H^{sh}})c_{ph}(T^{tu} - T^{sh}) + \frac{\pi D_i}{A^{sh}}U^{tu}(T^{tu} - T^{sh}) \tag{9}$$

The mass and energy balance for solid phase are written by:

$$\varepsilon_s c_t \frac{\partial y_{is}^{sh}}{\partial t} = k_{gi}(y_i^{sh} - y_{is}^{sh}) + \eta r_i \rho_B a, \quad i = 1, 2, \ldots, N-1 \tag{10}$$

$$\rho_B c_{ps}\frac{\partial T_s^{sh}}{\partial t} = a_v h_f(T^{sh} - T_s) + \rho_B a\sum_{i=1}^{N}\eta r_i(-\Delta H_{f,i}) \tag{11}$$

where y_i^{sh} and T_s^{sh} are the mole fraction and temperature of solid phase in shell side, respectively.

3.2.2. Tube side

Overall mass balance:

$$\frac{\partial c_t}{\partial t} = -\frac{1}{A_c}\frac{\partial F^{tu}}{\partial z} - \frac{\alpha_H}{A_c}(\sqrt{P_H^{tu}} - \sqrt{P_H^{sh}}) \tag{12}$$

where c_t and F^{tu} are total concentration and flow rate in tube side. The mass and energy balance equations for fluid phase are given:

$$c_t \frac{\partial y_i^{tu}}{\partial t} = -\frac{1}{A_c}\frac{\partial F_i^{sh}}{\partial z} - \frac{\alpha_H}{A_c}(\sqrt{P_H^{tu}} - \sqrt{P_H^{sh}}), \quad i = 1, 2, \ldots, N-1 \tag{13}$$

$$c_t c_{p_g}\frac{\partial T^{tu}}{\partial t} = -\frac{1}{A_c}C_{pg}\frac{\partial(F^{tu}T^{tu})}{\partial z} + \frac{\pi D_i}{A_c}U^{tu}(T^{sh} - T^{tu}) + \frac{\alpha_H}{A_c} \times (\sqrt{P_H^{tu}} - \sqrt{P_H^{sh}})C_{ph}(T^{sh} - T^{tu}) \tag{14}$$

The boundary conditions are as follow:

$$z = L; \quad y^{tu} = y_{if}, \quad T^{tu} = T_f \tag{15}$$

when $\alpha_H = 0$, the membrane is not permeable to hydrogen and the model is used for industrial two-stage system.

3.3. Deactivation model

The deactivation model of the $CuO/ZnO/Al_2O_3$ catalyst has been studied by several researchers, however, the suggested model by Hanken was found to be suitable for industrial applications [18]:

$$\exp\left(\frac{-E_d}{R}\left(\frac{1}{T} - \frac{1}{T_R}\right)\right)a^5\frac{da}{dt} = -K_d \tag{16}$$

where E_d, T_R and K_d are the activation energy, reference temperature and catalyst deactivation constant, respectively. These parameters are listed in Table 4 [18]. The above model has been fitted with industrial operating conditions and is the only case for simulation and modeling of industrial plants.

Table 4
Parameters of deactivation model [18].

Parameter	Value	Unit
K_d	0.00439	[h^{-1}]
E_d	91,270	[$J\,mol^{-1}$]
T_R	513	[K]

3.4. Hydrogen permeation in the Pd/Ag membrane

The flux of hydrogen permeating through the palladium membrane (j) depends on the difference in the hydrogen partial pressure on the two sides of the membrane. Here, the hydrogen permeation is determined assuming Sieverts' law:

$$j_H = \alpha_H(\sqrt{P_H^{tu}} - \sqrt{P_H^{sh}}) \quad (17)$$

Data for the diffusion of hydrogen through Pd–Ag membrane were determined experimentally. In Eqs. (7)–(12), α_H is hydrogen permeation rate constant and is defined as [19]:

$$\alpha_H = \frac{2\pi L\bar{P}}{\ln(R_o/R_i)} \quad (18)$$

where R_o, R_i candidate for outer and inner radius of Pd–Ag layer. Here, the hydrogen permeability through the Pd–Ag layer is determined assuming the Arrhenius law, which is a function of temperature as follows [20,21]:

$$\bar{P} = P_0 \exp\left(\frac{-E_p}{RT}\right) \quad (19)$$

where the pre-exponential factor P_0 above 200 °C is reported as 6.33×10^{-8} mol m^{-2} s^{-1} Pa$^{-1/2}$ and activation energy E_p is 15.7 kJ kmol^{-1} [20,21].

4. Numerical solution

The fundamental structure of the model is consisted of the partial derivative equations of mass and energy conservative rules of both the solid and fluid phase, which have to be coupled with the ordinary differential equation of the deactivation model, and also non-linear algebraic equations of the kinetic model and auxiliary correlations. The equations are solved using a two-stage approach consisting of a steady-state simulation stage followed by a dynamic solution stage. In order to solve the set of reactor model equations, a steady-state simulation has been used prior to a dynamic simulation and gives the initial values of the dynamic one.

4.1. Steady-state model solution

Steady-state model solution of the two-stage methanol reactor is carried out by setting all the time-variation of the states to zero and also considering a fresh catalytic bulk with the activity of unity. In this way, the initial conditions for temperature and concentration are determined for dynamic simulation.

At the steady-state condition, backward finite difference approximation was used to the system of ordinary differential-algebraic equations to solve the set of non-linear differential-algebraic equations (*NAEs*). These equations are a boundary value problem and solved using the shooting method. The water and gas-cooled reactors are divided into 14 and 16 sections, respectively, and the Gauss-Newton method is applied to solve the NAEs in each section. The procedure is as follows:

- The temperature (T_f) and molar flow rate (F_f) of feed synthesis gas stream are known, but temperature (T_{in}), molar flow rate (F_{in}) and composition (y_i) of the gas flow entering the catalyst bed of the first reactor are unknown.
- The values of these parameters (unknown parameters) are assumed.
- The equations of the first reactor are solved from up to down and for the second reactor, the same pattern is followed.
- The calculated values of temperature, molar flow rate and composition of fresh feed gas flow to the second reactor are compared with the actual values given as input of the problem.
- This procedure is repeated until the specified terminal values are obtained within a small convergence criterion.

4.2. Dynamic model solution

The results of the steady-state simulation are used as initial conditions for time integration of dynamic state equations in each node through the two-stage methanol synthesis reactor. The set of dynamic equations due to the deactivation model and conservation rules consists of simultaneous ordinary and partial differential equations, as well as the algebraic equations due to auxiliary correlations, kinetics and thermodynamics of the reaction system. The set of equations have been separated with respect to axial coordinate, and modified Rosenbrock formula of order 2 has been applied to the discrete equations in each node along the reactor to integrate the set of equations with respect to time. The process duration has been considered to be 1400 operating days.

5. Model validation

5.1. Steady-state model validation

The steady-state model was validated by comparing its results at time zero ($t = 0$) with plant data for a conventional two-stage methanol synthesis reactor ($\alpha_H = 0$) under the design specifications. Input data presented in Tables 1 and 2, respectively. The model results and data of the plant are tabulated in Table 5. It was observed that the steady-state model carried out acceptably well under industrial conditions and result of simulation with daily-real plant data were a good agreement.

5.2. Dynamic model validation

In order to verify the goodness of dynamic model, simulation results have been compared with the historical process data for single-stage reactor. The predicted results of production rate and the corresponding observed data of the plant are presented in Table 6. It was observed that, the model performed satisfactorily well under industrial conditions and a good agreement between daily-observed plant data and simulation data existed.

6. Results and discussion

A parametric analysis is performed to address the vital issues, such as the catalyst activity, temperature, CO mole fraction and removal rate profiles along the reactors. Fig. 4 shows a comparison of catalyst activity and temperature profiles, CO mole fraction and CO removal rate profiles along the conventional and membrane two-stage methanol synthesis reactor at 1st and 1400th days of operation. According to Eq. (16) catalyst activity is a function of temperature, thus local variation of temperature along the reactor causes local change in catalyst activity. As seen in parts (a and b),

Table 5
Comparison between model results with plant data for fresh catalyst.

Product condition	Plant	Predicted	Error %
Composition (mol%)			
CH_3OH	0.104	0.1023	−3.4
CO	0.0251	0.0228	−4.38
CO_2	0.0709	0.0764	−9.16
H_2O	0.0234	0.0211	−9.82
H_2	0.5519	0.5323	−3.55
N_2/Ar	0.0968	0.0905	−6.5
CH_4	0.114	0.103	−9.64
Temperature (K)	495	489.5	−1.2
CO removal rate (tons/day)	4465	4542.2	1.7

Table 6
Comparison between predicted methanol production rate and plant data.

Time (days)	Plant (tons/day)	Predicted (tons/day)	Error %
0	295.0	308.80	2.93
100	296.5	297.03	0.18
200	302.6	289.10	−4.46
300	284.3	283.09	−0.44
400	277.9	278.19	0.10
500	278.2	274.03	−1.50
600	253.0	270.41	6.88
700	274.0	267.19	−2.48
800	268.1	264.30	−1.65
900	275.5	261.67	−5.02
1000	274.6	259.25	−5.58
600	262.9	257.02	−2.24
1200	255.2	255.18	−0.05

the minimum activity level is observed near the entrance of first reactor that is exposed to higher temperature at all times. Also, the temperature profile in the water-cooled reactor of membrane system is higher than conventional up to 8 m in length because the feed synthesis gas in this reactor has a higher temperature than the reacting gas mixture in the gas-cooled reactor. These parts also demonstrate that the second reactor of membrane system due to addition of hydrogen to the reacting materials has a lower temperature. Therefore, the temperature profile along the membrane two-stage reactor is more desirable than the conventional reactor. This desired lower temperature improves both the catalyst activity and equilibrium constant which results in a shift of the equilibrium conversion to a higher value. The favorable thermodynamic equilibrium at lower temperatures and H_2 permeation along the membrane two-stage methanol reactor are the main reasons for obtaining the higher CO removal rate in comparison with the conventional system at any time of operation as shown in parts (c) and (d).

Fig. 5(a and b) demonstrates CO mole fraction and CO removal rate versus length and time for membrane two-stage methanol reactor. CO mole fraction decreases along the reactor and increases with time. Catalyst deactivation is the major reason for increase in CO mole fraction and reduction in CO removal rate as time passes.

Fig. 6 shows that the catalyst deactivation in the membrane reactor due to lower temperature is less than in the conventional two-stage reactor.

Fig. 7 illustrates CO mole fraction and CO removal rate profiles along the membrane two-stage methanol synthesis reactor at three different times of operation. Between the 1st and 1400th days of operation, catalyst deactivation leads to a conversion reduction. It is shown in this figure that, mole fraction of CO in product stream increases and CO removal rate decreases as times passes.

Fig. 8 shows the CO mole fraction and CO removal rate over a period of 1400 operating days for both types of methanol synthesis reactor systems. As can be seen, there is a considerable increase in amount of CO removal rate in membrane two-stage reactor.

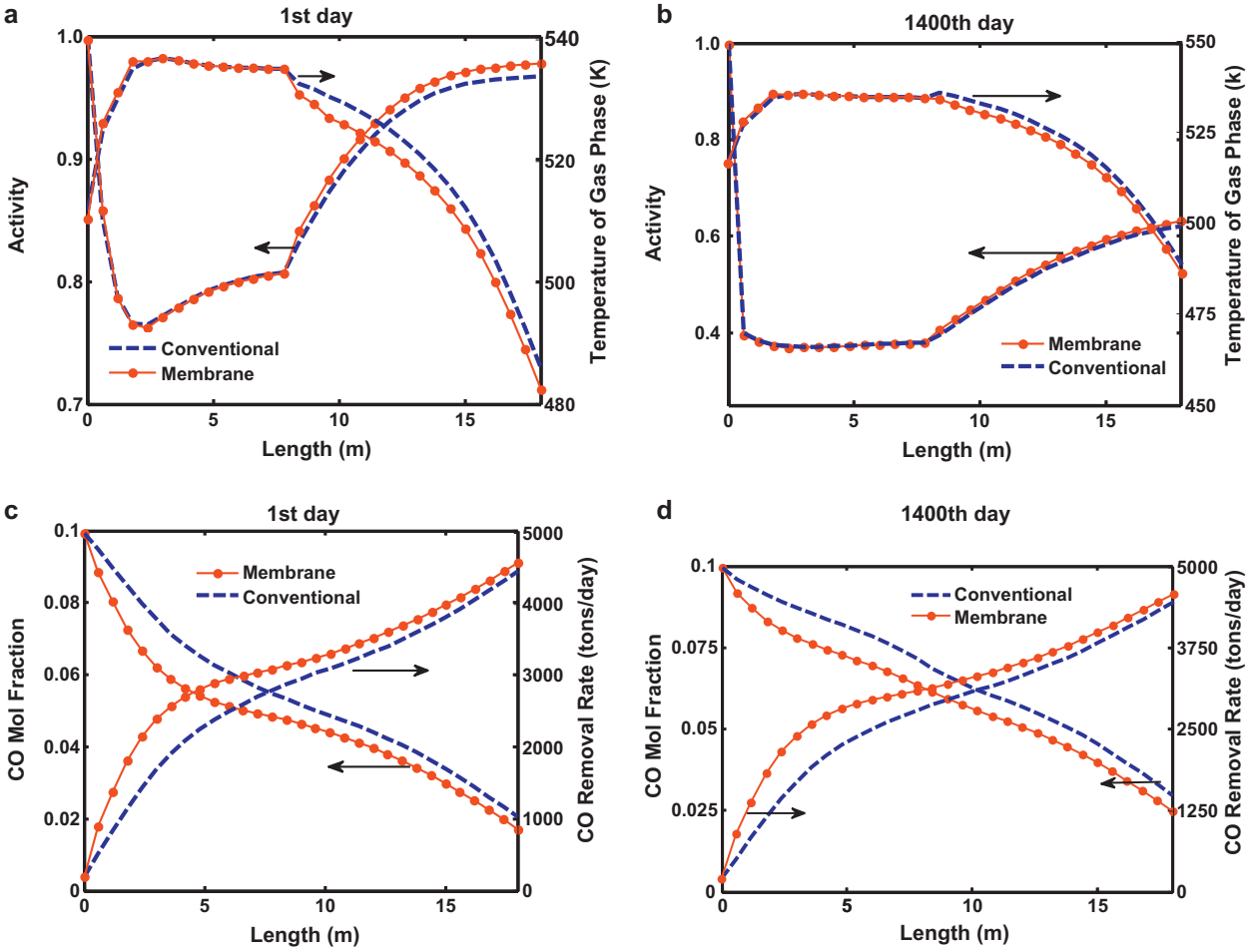

Fig. 4. Comparison of (a and b) catalyst activity and temperature profiles and (c and d) CO mole fraction and CO removal rate profiles along the conventional and membrane two-stage methanol synthesis reactors for 1st and 1400th days of operation.

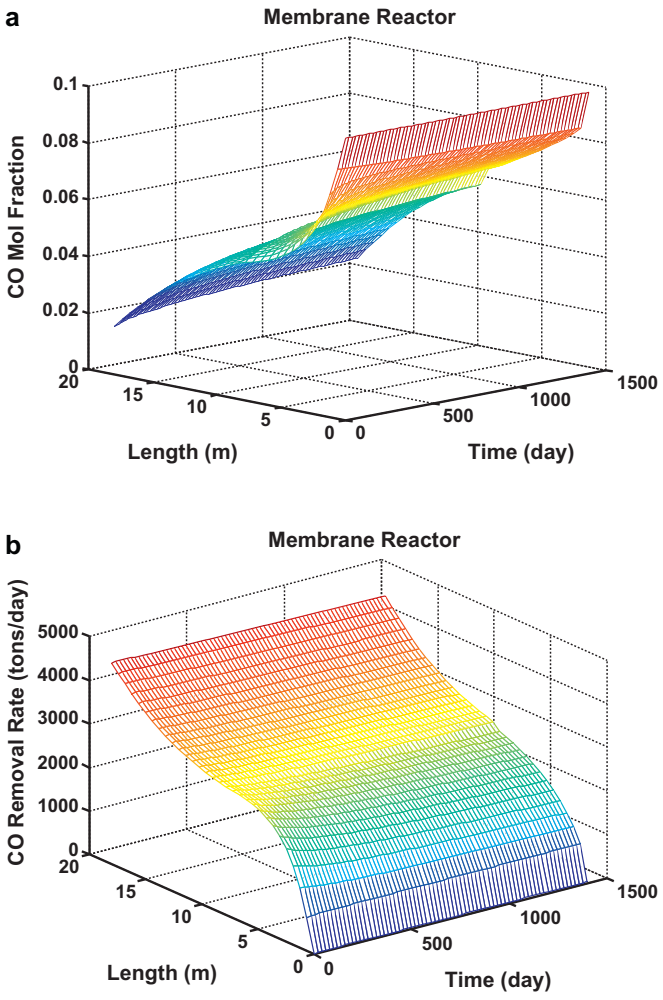

Fig. 5. Profiles of (a) CO mole fraction and (b) CO removal rate versus time and length in membrane two-stage methanol reactor.

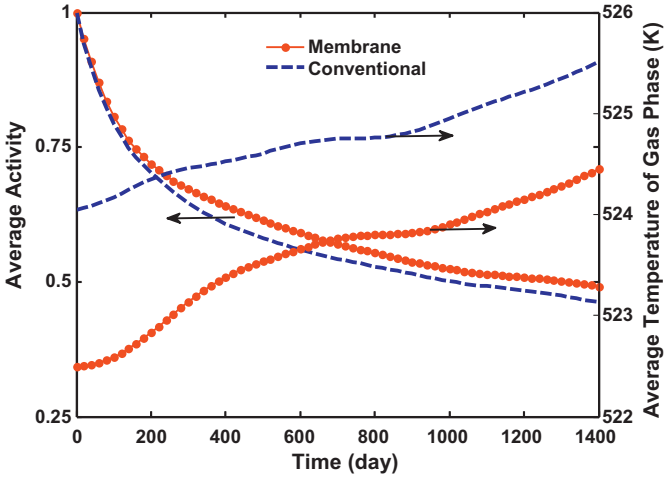

Fig. 6. Comparison of the average activity and average temperature at a period of 1400 days of operating for conventional and membrane two-stage reactors.

7. Conclusion

Carbon monoxide is the most abundant and widely distributed air pollutant. The catalytic hydrogenation of CO to methanol represents an effective method for reducing the harmful effects of this poisonous gas. In this work, a Pd–Ag membrane was used in the second reactor of a two-stage methanol synthesis reactor for enhancement of CO removal and its performance was compared with a conventional two-stage methanol synthesis reactor. Potential possibilities of the membrane were examined using one-dimensional heterogeneous model to obtain the necessary comparative estimates. A comparison of the catalyst temperature profiles along the length of the reactor in both systems shows that in the membrane system, temperature profile of the catalyst bed is very desirable. This advantage leads to:

- Longer catalyst lifetime due to higher activity along the reactor.
- High level of catalyst activity in the gas-cooled reactor results in a higher CO conversion which means higher CO removal rate.

The results of this study show that the application of membrane two-stage methanol synthesis reactor is an attractive system for improvement of CO conversion to methanol and reducing CO emissions into the atmosphere.

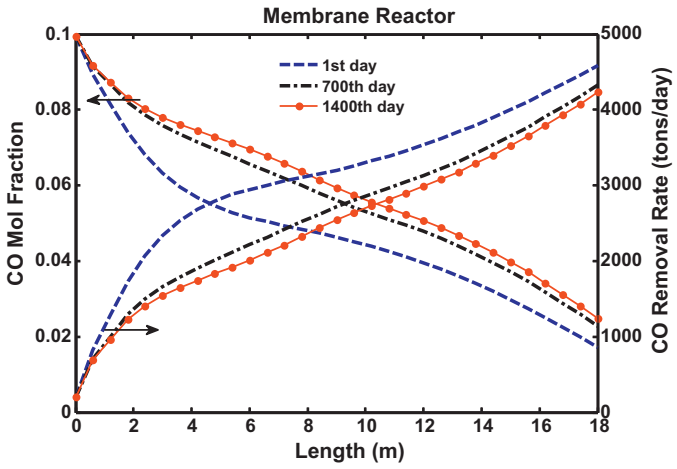

Fig. 7. Profiles of CO mole fraction and CO removal rate along the membrane reactor at 1st, 700th, and 1400th days.

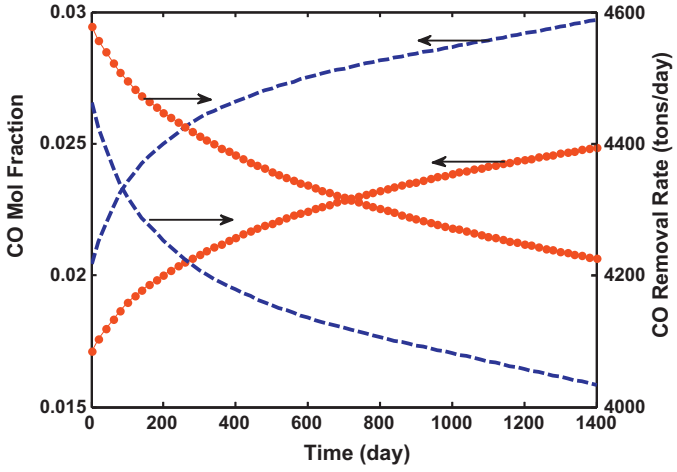

Fig. 8. Comparison of CO mole fraction and CO removal rate at a period of 1400 operating days for conventional and membrane two-stage reactors.

Acknowledgement

The authors would like to thank Zagross Petrochemical Company of Iran for providing valuable operating data.

Appendix A. Reaction kinetics

A.1. Reaction kinetics

In the methanol synthesis, three overall reactions are possible: hydrogenation of carbon monoxide, hydrogenation of carbon dioxide and reverse water–gas shift reaction, which follow as:

$$CO + 2H_2 \leftrightarrow CH_3OH, \qquad \Delta H_{298} = -90.55\ \text{kJ mol}^{-1} \tag{A.1}$$

$$CO_2 + H_2 \leftrightarrow CO + H_2O, \qquad \Delta H_{298} = +41.12\ \text{kJ mol}^{-1} \tag{A.2}$$

$$CO_2 + 3H_2 \leftrightarrow CH_3OH + H_2O, \qquad \Delta H_{298} = -49.43\ \text{kJ mol}^{-1} \tag{A.3}$$

Reactions (A.1)–(A.3) are not independent so that one is a linear combination of the other ones. In the current work, the rate expressions have been selected from Graaf et al. [22]. The rate equations combined with the equilibrium rate constants [23] provide enough information about kinetics of methanol synthesis. The correspondent rate expressions due to the hydrogenation of CO, CO_2 and the reversed water–gas shift reactions are:

$$r_1 = \frac{k_1 K_{CO}[f_{CO} {f_{H_2}}^{3/2} - f_{CH_3OH}/({f_{H_2}}^{1/2} K_{p1})]}{(1 + K_{CO} f_{CO} + K_{CO_2} f_{CO_2})[{f_{H_2}}^{1/2} + (K_{H_2O}/{K_{H_2}}^{1/2}) f_{H_2O}]} \tag{A.4}$$

$$r_2 = \frac{k_3 K_{CO_2}[f_{CO_2} f_{H_2} - f_{H_2O} f_{CO}/K_{p3}]}{(1 + K_{CO} f_{CO} + K_{CO_2} f_{CO_2})[f_{H_2}^{1/2} + (K_{H_2O}/{K_{H_2}}^{1/2}) f_{H_2O}]} \tag{A.5}$$

$$r_3 = \frac{k_2 K_{CO_2}[f_{CO_2} f_{H_2}^{3/2} - f_{CH_3OH} f_{H_2O}/(f_{H_2}^{3/2} K_{p2})]}{(1 + K_{CO} f_{CO} + K_{CO_2} f_{CO_2})[f_{H_2}^{1/2} + (K_{H_2O}/K_{H_2}^{1/2}) f_{H_2O}]} \tag{A.6}$$

The reaction rate constants, adsorption equilibrium constants and reaction equilibrium constants which occur in the formulation of kinetic expressions are tabulated in Tables A.1–A.3, respectively.

Table A.1
Reaction rate constants [22].

$K = A\exp(\frac{B}{RT})$	A	B
K_1	$(4.89 \pm 0.29) \times 10^7$	$-113{,}000 \pm 300$
K_2	$(9.64 \pm 7.30) \times 10^7$	$-152{,}900 \pm 11{,}800$
K_3	$(1.09 \pm 0.07) \times 10^7$	$-87{,}500 \pm 300$

Table A.2
Adsorption equilibrium constants [22].

$K = A\exp(\frac{B}{RT})$	A	B
K_{CO}	$(2.16 \pm 0.44) \times 10^{-5}$	$46{,}800 \pm 800$
K_{CO_2}	$(7.05 \pm 1.39) \times 10^{-7}$	$61{,}700 \pm 800$
$(K_{H_2O}/K_{H_2}^{1/2})$	$(6.37 \pm 2.88) \times 10^{-9}$	$84{,}000 \pm 1400$

Table A.3
Reaction equilibrium constants [22].

$K = A\exp(\frac{B}{RT})$	A	B
K_{p1}	5139	12.621
K_{p2}	−2073	−2.029
K_{p3}	3066	10.592

Appendix B. Auxiliary correlations

B.1. Mass transfer correlations

In the current work, mass transfer coefficients for the components have been taken from Cusler [24]. These are mass transfer coefficients between gas phase and solid phase.

$$k_{gi} = 1.17 Re^{-0.42} {Sc_i}^{-0.67} u_g \times 10^3 \tag{B.1}$$

where the Reynolds and Schmidt numbers have been defined as:

$$Re = \frac{2R_p u_g}{\mu} \tag{B.2}$$

$$Sc_i = \frac{\mu}{\rho D^i \times 10^{-4}} \tag{B.3}$$

And the diffusivity of component i in the gas mixture is given by [25].

$$D_{im} = \frac{1 - y_i}{\sum_{i=j} y_i / D_{ij}} \tag{B.4}$$

And also the binary diffusivities are calculated using the Fuller–Schetter–Giddins equation that is reported by Reid et al. [26]. In the following Fuller–Schetter–Giddins correlation, ν_{ci}, M_i are the critical volume and molecular weight of component i which are reported in Table B.1 [27].

$$D_{ij} = \frac{10^{-7} T^{3/2} \sqrt{(1/M_i) + (1/M_j)}}{P(\nu_{ci}^{3/2} + \nu_{cj}^{3/2})^2} \tag{B.5}$$

Knowing the fact that diffusion path length along the pores is greater than the measurable thickness of the pellet, for the effective diffusivity in the catalyst pore, correction should be implemented due to the structure of the catalyst. The correction factor is ratio of catalyst void fraction to the tortuosity of the catalyst (τ).

B.2. Heat transfer correlations

The overall heat transfer coefficient between circulating boiling water of the shell side and bulk of the gas phase in the tube side is given by the following correlation.

$$\frac{1}{U_{shell}} = \frac{1}{h_i} + \frac{A_i \ln(D_o/D_i)}{2\pi L K_w} + \frac{A_i}{A_o}\frac{1}{h_o} \tag{B.6}$$

where h_i is the heat transfer coefficient between the gas phase and reactor wall and is obtained by the following correlation [28].

$$\frac{h_i}{C_p \rho \mu}\left(\frac{C_p \mu}{K}\right)^{2/3} = \frac{0.458}{\varepsilon_B}\left(\frac{\rho u d_p}{\mu}\right)^{-0.407} \tag{B.7}$$

where in the above equation, u is superficial velocity of gas and the other parameters are those of bulk gas phase and d_p is the equivalent catalyst diameter, K is thermal conductivity of gas, ρ, μ

Table B.1
Molecular weight and critical volume of the components.

Component	M_i (g mol^{-1})	ν_{ci} ($\times 10^6$ m^3 mol^{-1})
CH_3OH	32.04	118.0
CO	28.01	18.0
CO_2	44.01	94.0
H_2O	18.02	56.0
H_2	2.02	6.1
CH_4	16.04	99.0
N_2	28.01	18.5

are density and viscosity of gas, respectively and ε_B is void fraction of catalyst bed.

In Eq. (B.6), h_o is the heat transfer coefficient of boiling water in the shell side which is estimated by the following equation [29]:

$$h_o = 7.96(T - T_{sat})^3 \left(\frac{P}{P_a}\right)^{0.4} \quad \text{(B.8)}$$

T and P are temperature and pressure of boiling water in the shell side, T_{sat} is the saturated temperature of boiling water at the operating pressure of shell side and P_a is the atmospheric pressure. The last term of the above equation has been considered due to effect of pressure on the boiling heat transfer coefficient. For the heat transfer coefficient between bulk gas phase and solid phase h_f, Eq. (B.7) is applicable.

Appendix C. Nomenclature

A_c cross-section area of each tube (m^2)
A_i inner area of each tube (m^2)
A_o outside area of each tube (m^2)
A^{sh} cross-section area of shell (m^2)
α activity of catalyst
a_v specific surface area of catalyst pellet ($m^2\ m^{-3}$)
c_{pg} specific heat of the gas at constant pressure ($J\ mol^{-1}\ K^{-1}$)
c_{ph} specific heat of the hydrogen at constant pressure ($J\ mol^{-1}\ K^{-1}$)
c_{ps} specific heat of the catalyst at constant pressure ($J\ mol^{-1}\ K^{-1}$)
c_t total concentration ($mol\ m^{-3}$)
D reactor diameter (m)
D_i tube inside diameter (m)
D_{ij} binary diffusion coefficient of component i in j ($m^2\ s^{-1}$)
D_m^i diffusion coefficient of component i in the mixture ($m^2\ s^{-1}$)
D_o tube outside diameter (m)
d_p particle diameter (m)
E_d activation energy used in the deactivation model ($J\ mol^{-1}$)
F^{sh} total molar flow in shell side ($mol\ s^{-1}$)
F^{tu} total molar flow per tube ($mol\ s^{-1}$)
f_i partial fugacity of component i (bar)
h_f gas-catalyst heat transfer coefficient ($W\ m^{-2}\ K^{-1}$)
h_i heat transfer coefficient between fluid phase and reactor wall ($W\ m^{-2}\ K^{-1}$)
h_o heat transfer coefficient between coolant stream and reactor wall ($W\ m^{-2}\ K^{-1}$)
K conductivity of fluid phase ($W\ m^{-1}\ K^{-1}$)
K_d deactivation model parameter constant (s^{-1})
K_i adsorption equilibrium constant for component i (bar^{-1})
K_{pi} equilibrium constant based on partial pressure for component i
K_w thermal conductivity of reactor wall ($W\ m^{-1}\ K^{-1}$)
k_1 reaction rate constant for the 1st rate equation ($mol\ kg^{-1}\ s^{-1}\ bar^{-1/2}$)
k_2 reaction rate constant for the 2nd rate equation ($mol\ kg^{-1}\ s^{-1}\ bar^{-1/2}$)
k_3 reaction rate constant for the 3rd rate equation ($mol\ kg^{-1}\ s^{-1}\ bar^{-1/2}$)
k_{gi} mass transfer coefficient for component i ($m\ s^{-1}$)
L length of reactor (m)
M_i molecular weight of component i ($g\ mol^{-1}$)
N number of components
N_i molar flux ($mol\ s^{-1}\ m^{-2}$)
P total pressure (bar)
P_a atmospheric pressure (bar)
P_H^{tu} tube side pressure (bar)
P_H^{sh} shell side pressure (bar)
$\bar{P}$ permeability of hydrogen through Pd–Ag layer ($mol\ m^{-1}\ s^{-1}\ Pa^{-1/2}$)
P_0 pre-exponential factor of hydrogen permeability ($mol\ m^{-1}\ s^{-1}\ Pa^{-1/2}$)
R universal gas constant ($J\ mol^{-1}\ K^{-1}$)
R_e Reynolds number
R_i inner radius of Pd–Ag layer (m)
R_o outer radius of Pd–Ag layer (m)
r_i reaction rate of component i ($mol\ kg^{-1}\ s^{-1}$)
r_1 rate of reaction for hydrogenation of CO ($mol\ kg^{-1}\ s^{-1}$)
r_2 rate of reaction for hydrogenation of CO_2 ($mol\ kg^{-1}\ s^{-1}$)
r_3 reversed water–gas shift reaction ($mol\ kg^{-1}\ s^{-1}$)
Sc_i Schmidt number of component i
T bulk gas phase temperature (K)
T_R reference temperature used in the deactivation model (K)
T_s temperature of solid phase (K)
T_{sat} saturated temperature of boiling water at operating pressure (K)
T^{sh} temperature of coolant stream, in first reactor (K)
T^{tu} temperature of coolant stream, in second reactor (K)
t time (s)
U^{sh} overall heat transfer coefficient between coolant and process streams ($W\ m^{-2}\ K^{-1}$)
U superficial velocity of fluid phase ($m\ s^{-1}$)
u_g linear velocity of fluid phase ($m\ s^{-1}$)
y_i^{sh} mole fraction of component i in the fluid phase in shell ($mol\ mol^{-1}$)
y_{is}^{sh} mole fraction of component i in the solid phase in shell ($mol\ mol^{-1}$)
y_i^{tu} mole fraction of component i in the fluid phase in tube side ($mol\ mol^{-1}$)
y_{is}^{tu} mole fraction of component i in the solid phase in tube side ($mol\ mol^{-1}$)
z axial reactor coordinate (m)

Greek letters

α_H hydrogen permeation rate constant ($mol\ m^{-1}\ s^{-1}\ Pa^{-1/2}$)
$\Delta H_{f,i}$ enthalpy of formation of component i ($J\ mol^{-1}$)
ΔH_{298} enthalpy of reaction at 298 K ($J\ mol^{-1}$)
ε_B void fraction of catalytic bed
ε_s void fraction of catalyst
μ viscosity of fluid phase ($kg\ m^{-1}\ s^{-1}$)
ν stoichiometric coefficient
ν_{ci} critical volume of component i ($cm^3\ mol^{-1}$)
ρ density of fluid phase ($kg\ m^{-3}$)
ρ_B density of catalytic bed ($kg\ m^{-3}$)
ρ_s density of catalyst ($kg\ m^{-3}$)
η catalyst effectiveness factor
τ tortuosity of catalyst
Ω auxiliary variable
Δ thickness of membrane (m)

Superscripts and subscripts

i component i
f feed conditions
p permeation side
in inlet conditions
out outlet conditions
k reaction number index (1, 2 or 3)

s	at catalyst surface
sh	shell side
ss	initial conditions (i.e., steady-state condition)
tu	tube side

References

[1] Ch. Bruhl, P.J. Crutzen, Chemosphere-Global Change Sci. 1 (1999) 249.
[2] J.M. Han, H.Y. Shin, B.M. Min, K.H. Han, A. Cho, J. Ind. Eng. Chem. 15 (2009) 212.
[3] S.H. Kang, J.W. Bae, P.S.S. Prasad, J.H. Oh, K.W. Jun, S.L. Song, K.S. Min, J. Ind. Eng. Chem. 15 (2009) 665.
[4] A. Neramittagapong, N. Grisdanurak, S. Neramittagapong, J. Ind. Eng. Chem. 14 (2008) 429.
[5] J.J. Park, Y. Shin, J.H. Oh, C.H. Chung, Y.J. Huh, S. Haam, J. Ind. Eng. Chem. 15 (2009) 618.
[6] J.P. Breen, J.R.H. Ross, Catal. Today 51 (1999) 521.
[7] P.J.A. Tijm, F.J. Waller, D.M. Brown, Appl. Catal. A: Gen. 221 (2001) 275.
[8] M.R. Rahimpour, S. Ghader, Chem. Eng. Process. 43 (2004) 1181.
[9] M.R. Rahimpour, M. Lotfinejad, Chem. Eng. Technol. 30 (2007) 1062.
[10] D.S. Kim, D.H. Kim, B.S. Lee, G.Y. Moon, H.K. Lee, N.S. Yong, J.W. Rhim, J. Ind. Eng. Chem. 15 (2009) 393.
[11] M.R. Rahimpour, A. Asgari, J. Hazard. Mater. 153 (2008) 557.
[12] F. Roa, M.J. Block, J.D. Way, Desalination 147 (2002) 411.
[13] J. Shu, B.P.A. Grandjean, A.V. Neste, S. Kaliaguine, Can. J. Chem. Eng. 69 (1991) 1060.
[14] Y.M. Lin, M.H. Rei, Catal. Today 67 (2001) 77.
[15] M.R. Rahimpour, S. Ghader, Chem. Eng. Technol. 26 (2003) 902.
[16] R.E. Buxbaum, A.B. Kinney, Ind. Eng. Chem. Res. 35 (1996) 530.
[17] R. Dittmeyer, V. Höllein, K. Daub, J. Mol. Catal. A: Chem. 173 (2001) 135.
[18] L. Hanken, Master's thesis, The Norwegian University of Science and Technology, 1995.
[19] S. Hara, W.C. Xu, K. Sakaki, N. Itoh, Ind. Eng. Chem. Res. 38 (1999) 488.
[20] G. Barbieiri, F. Di. Maio, Ind. Eng. Chem. Res. 36 (1997) 2121.
[21] J. Shu, B.P.I. Grandjean, S. Kaliaguine, Appl. Catal. A: Gen. 119 (1994) 305.
[22] G.H. Graaf, H. Scholtens, E.J. Stamhuis, A.A.C.M. Beenackers, Chem. Eng. Sci. 45 (1990) 773.
[23] G.H. Graaf, P.J.J.M. Sijtsema, E.J. Stamhuis, G.E.H. Joosten, Chem. Eng. Sci. 41 (1986) 2883.
[24] E.L. Cussler, Diffusion—Mass Transfer in Fluid Systems, Cambridge University Press, Cambridge, 1984.
[25] C.R. Wilke, Chem. Eng. Prog. 45 (1949) 218.
[26] R.C. Reid, T.K. Sherwood, J. Prausnitz, The Properties of Gases and Liquids, third ed., McGraw-Hill, New York, 1977.
[27] F. Hartig, F.J. Keil, Ind. Eng. Chem. Res. 32 (1993) 424.
[28] J.M. Smith, Chemical Engineering Kinetics, McGraw-Hill, New York, 1980.
[29] J.P. Holman, Heat Transfer, McGraw-Hill, New York, 1989.